Dalton Transactions

Controlled Synthesis of Photoresponsive Bismuthinite (Bi_2S_3) Nanostructures Mediated Through a New 1D Bismuth-pyrimidylthiolate Coordination Polymer as Molecular Precursor

Journal:	*Dalton Transactions*
Manuscript ID	DT-ART-07-2023-002143.R2
Article Type:	Paper
Date Submitted by the Author:	31-Aug-2023
Complete List of Authors:	Kulkarni, Atharva; K J Somaiya College of Arts and Commerce Karmakar, Gourab; Bhabha Atomic Research Centre, Chemistry Shah, Alpa; Bhabha Atomic Research Centre, Chemistry Nigam, Sandeep; Bhabha Atomic Research Centre, Chemistry Division Kumbhare, Gayatri; KJ Somaiya College of Engineering Tyagi, Adish; Bhabha Atomic Research Centre, Chemistry Butcher, Raymond J ; Howard University Chauhan, Rohit; K J Somaiya College of Science and Commerce, Chemistry Kumar, N Naveen; Bhabha Atomic Research Centre, Material Science Division

Controlled Synthesis of Photoresponsive Bismuthinite (Bi_2S_3) Nanostructures Mediated Through a New 1D Bismuth-pyrimidylthiolate Coordination Polymer as Molecular Precursor

Atharva Yeshwant Kulkarni,[#a] Gourab Karmakar,[#b,c] Alpa Y. Shah,[b] Sandeep Nigam,[b,c] Gayatri Kumbhare,[a] Adish Tyagi,[b,c]* Raymond J. Butcher,[d] Rohit Singh Chauhan,[a]* N. Naveen Kumar[e]

[a]*Department of Chemistry, K. J. Somaiya College of Science and Commerce, Vidyavihar, Mumbai 400077, India.*

[b]*Chemistry Division, Bhabha Atomic Research Centre, Mumbai 400085, Homi Bhabha National Institute, Mumbai 400094, India*

[c]*Homi Bhabha National Institute, Anushaktinagar, Mumbai- 400094, India*

[d]*Department of Chemistry, Howard University, Washington DC, 20059, United States.*

[e]*Materials Science Division, Bhabha Atomic Research Centre, Mumbai – 400085, India*

[#]These authors contributed equally.

Email: tyagia@barc.gov.in, rohit.chauhan@somaiya.edu.

Abstract

Bismuthinite (Bi_2S_3) nanostructures have garnered significant interest due to their appealing photoresponsivity which positioned them as an attractive choice for energy conversion application. However, to utilize their full potential, a simple and economically viable method of preparation is highly desirable. Herein, we present the synthesis and characterization including structural elucidation of new air and moisture stable bismuth-pyrimidylthiolate complex. This complex serves as an efficient single source molecular precursor for the facile preparation of phase pure Bi_2S_3 nanostructures. Powder X-ray diffraction (PXRD), Raman spectroscopy, electron dispersive spectroscopy (EDS) and electron microscopic techniques were used to assess the crystal structure, phase purity, elemental composition and morphology of the as-prepared nanostructures. The study also revealed the profound effect of temperature and growth duration on the crystallinity, phase formation and morphology of nanostructures. The optical band gap of the nanostructures was tuned within the range of 1.9 – 2.3 eV, which is blue shifted with respect to bulk bandgap and suitable for photovoltaic applications. Liquid junction photo-electrochemical cell fabricated from the as-prepared Bi_2S_3 nanostructure exhibit efficient photoresponsivity

and good photo-stability, which project them as promising candidates for alternative low-cost photon absorber materials.

Introduction

Ever growing global energy crisis and pressing need of environmental governance have intensified the quest for sustainable and efficient solar energy conversion technologies. Photovoltaic cells play a pivotal role in this direction.[1] Developing efficient solar absorber materials which constitute the heart of solar cells is currently an important research area. In this context, metal chalcogenides offered a fertile chemical space for exploration.[2] While commercialized materials like $Cu_2(In, Ga)Se_2$ and CdTe have shown promise, challenges such as scarcity, toxicity, and structural complexities necessitate the exploration of alternative chalcogenides.[3] Recently, group-V metal chalcogenides (V-VI materials), particularly bismuthinite (Bi_2S_3) have emerged as a promising photon absorber material due to their exciting electrical and optical properties. Bismuthinite possess several key attributes such as narrow band gap, high absorption coefficient of the order 10^5 cm^{-1} and good carrier mobility, which make it an intriguing material for energy conversion applications.[4] Bi_2S_3 is stibinite structured and crystallizes in the orthorhombic P_{nma} space group and can be described as a layered structure which offers opportunity of exfoliation down to monolayer.[5] With a band gap ranging from 1.4 to 1.7 eV, Bi_2S_3 holds potential for generating high open circuit voltage, making it an attractive light absorber material for top cells in tandem solar cells. Furthermore, being restriction of hazardous substances complaint and benefited from non-toxic and earth-abundant constituent elements, Bi_2S_3 pose as a promising candidate for sustainable solar cells.[6]

To fully exploit the potential of Bi_2S_3 in solar cell application, cost effective and scalable synthetic protocol for nanometric Bi_2S_3 is highly desirable. Various solution assisted and solventless synthetic routes including solvothermal,[7] hydrothermal,[8] sonochemical,[9] microwave assisted,[10] green synthesis,[11] etc. have been explored for the synthesis of Bi_2S_3 nanostructures. It is observed that most of these methods employ dual precursor route wherein a bismuth source ($Bi(NO_3)_3.5H_2O$, BiI_3, etc.) combines with a suitable sulfur source (elemental S, H_2S, Na_2S, thiourea, hexamethyldisilathiane, etc.) to produce Bi_2S_3. However, dual precursor route often employ precursors which are either sensitive (BiI_3, Na_2S, hexamethyldisilathiane) or toxic (H_2S) which severely limits the wide scale utility of the final

material.[12] In light of the limitations associated with dual precursor route, single source precursor (SSP) has gained significant attraction. SSP route involves a precursor molecule that contains all the desired constituent elements having preformed bond between them. This approach ensures low decomposition temperature, phase purity of final product and high reproducibility of experimental results.[12] Moreover, molecular precursor offer several distinct advantages over dual precursor route in terms of lower defect concentration and better control over their morphology and electronic properties.[13] These appealing features of SSP coupled with promising applications of Bi_2S_3 have ignited extensive research for the development of SSP for Bi_2S_3. However, only few suitable precursors have been identified and that too mainly derived from xanthates, dithiocarbamates and dithiophosphates.[13-22] In recent times, coordination polymers have gained significant attention as versatile SSPs, enabling the synthesis of advanced materials with unique morphologies that are hard to realize in conventional synthetic method.[23,24] The coordination polymer allows control release of the constituent element during thermal decomposition which provides access to nanomaterials of uniform size and morphology. As a result of this, when thermolyzed under appropriate conditions, they convert into materials with unusual morphology and chemical compositions. Moreover, due to the porous nature of the coordination polymers, they sometimes retain the structural exoskeleton after decomposition, which lead to porous nanomaterials with distinctive properties in several cases.[23] The most distinctive feature of coordination polymers is the possibility of tuning their thermal stability by the choice of metal ions/ clusters and linkers. Consequently, various functional nanomaterials/composites and heterostructures can be obtained depending upon the nature of precursor and decomposition conditions.[23] Depending on the countless number and type of coordination polymers, decomposition routes, reaction time, media etc., a plethora of different nanomaterial/composites/heterostructures can be isolated.[24] Thus, this field offer limitless potential for synthesizing assorted functional nanomaterials for energy and environmental application. However, surprisingly coordination polymer driven synthesis of Bi_2S_3 largely remains elusive.

Considering the importance of SSP for Bi_2S_3 and continuing our ongoing endeavour towards developing novel precursors for functional metal chalcogenides nanostructures,[25-28] in this report we present a 1D bismuth-pyrimidylthiolate coordination polymer, which served as an efficient precursor for the synthesis of Bi_2S_3 nanorods. For the preparation of

coordination polymer, we employed internally functionalized hemilabile 4,6-dimethylpyrimidyl-2-thiolate ligand. Steric congestion exerted by the two-hanging methyl group compels the pyrimidyl thiolate rings to adopt different coordination behaviour viz. chelating as well as bridging. This intriguing structural feature assists the growth of ID-polymeric chain of the complex. Further, the thermal transformation of this complex into nanostructures and variation of their crystallinity, morphology and bandgap as a function of reaction time and temperature have been investigated. In this work, it has also been demonstrated that utilization of this precursor presents a robust synthetic pathway for the formation of highly photoresponsive Bi_2S_3 nanostructures. The results of this work are described herein.

Results and Discussion

Synthesis and X-ray crystallography

Treatment of $Bi(NO_3)_3{\cdot}5H_2O$ with the thiolate ligand 4,6-Me_2pymS$^-$ in 1:3 molar ratio resulted into the title complex **1** (Scheme 1). The crystalline complex was characterized by PXRD analysis at room temperature to understand it's phase purity (Fig. 1). The reflections match exactly with the simulated PXRD pattern of the complex as generated from single crystal data. Diffraction quality single crystals of title complex were obtained by slow evaporation of solvent from the reaction mixture. The molecular structure of complex $[Bi(4,6\text{-}Me_2pymS)_3]_n$ (**1**) with the atomic numbering scheme is shown in Fig. 1a. Crystallographic and structural determination data along with the refinement parameters are given in Table 1 and the selected inter-atomic parameters of are summarized in Supplementary Information Table 1.

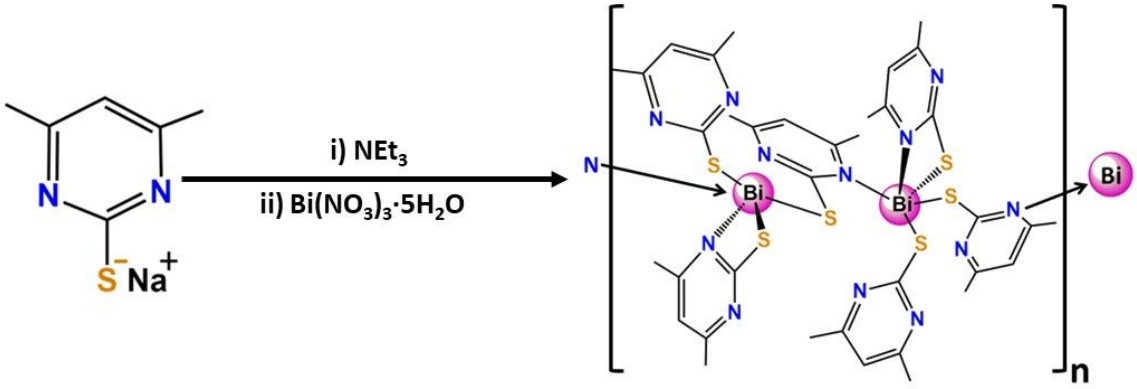

Scheme 1. Schematic diagram for the synthesis of $[Bi(4,6\text{-}Me_2pymS)_3]_n$ (**1**).

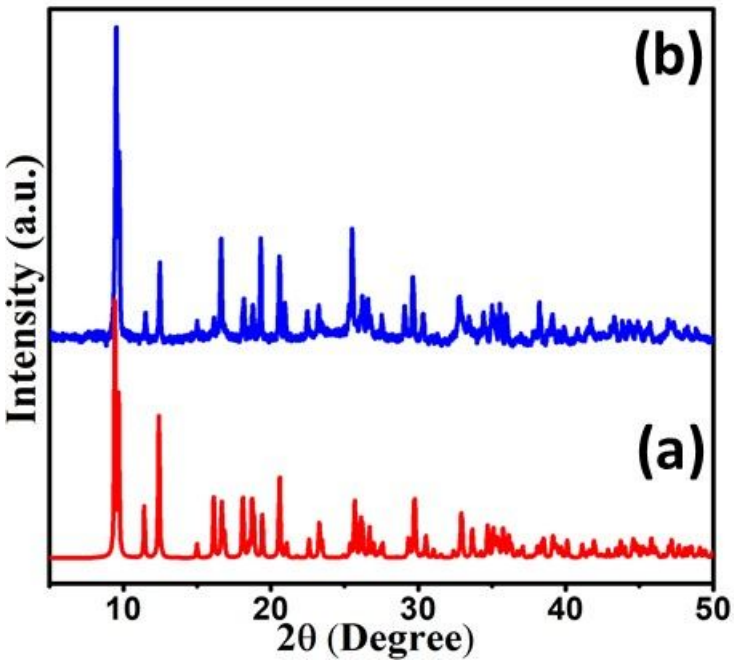

Fig. 1. (a) simulated XRD pattern of $[Bi(4,6\text{-}Me_2pymS)_3]_n$ (**1**) generated from single crystal data and (b) X-ray powder diffraction (PXRD) pattern of $[Bi(4,6\text{-}Me_2pymS)_3]_n$ (**1**).

The title complex **1** crystallizes in toluene-methanol mixture with orthorhombic crystal system having space group $P\,2_1\,2_1\,2_1$. The asymmetric unit consists of one Bi(III) and three ligand units and the unit cell contains four such molecules (Z = 4). The solid-state structure of **1** revealed it to be a 1D coordination polymer, construction of which is realized by the assembly of the asymmetric unit $[Bi(4,6\text{-}Me_2pymS)_3]$ (Fig. 2a). The structure comprises of one-dimensional polymeric wavy chains of the repeating unit $[Bi(4,6\text{-}Me_2pymS)_3]$ propagating through crystallographic *b*-axis (Fig. 2b). Interestingly the coordination behaviour of the three ligand moieties to the Bi centre is different. While one of the pyrimidine rings is attached to Bi in a chelated fashion through exocyclic sulfur S(1A) and nitrogen N(2A) atoms in κ-*N,S* fashion, forming one four-membered metallacyclic ring, another ligand coordinates the central metal ion through sulfur atom only (S1B), *i.e.*, in a non-chelating manner. The third ligand exhibits a peculiar bridging behaviour, where it binds with one Bi centre through it's sulfur donor site (S1C) and whereas the nitrogen N(2C) atom of ligand is coordinated to Bi atom of another asymmetric unit. This differential bonding fashion of the three ligands leads to a 1D $[Bi(\kappa\text{-S,N-pymS})(pymS)(\mu\text{-S,N-pymS})]_n$ polymeric chain. These 1D chain assemblies are held in the 3D structure through a complex network of

short contacts as presented in Fig. 2c. The central metal ion adopts distorted square pyramidal geometry where the coordination core is defined through "S3N" donor atoms. One of the reasons for the distortion in the geometry is the presence of stereochemically active lone pair on bismuth. The sulfur atom S1A resides at the axial position whereas the equatorial position is occupied by the two non-chelating ligands through sulfur (S1B, S1C) and nitrogen atoms N(2A), N(2C). The bond angles S(1A)-Bi-S(1B) = 79.46(15), S(1B)-Bi-S(1C) = 87.758(15), S(1C)-Bi-S(1A) = 87.168(16), N(2A)-Bi-S(1A) = 58.98(3) are deviated from ideal value of 90° which can be considered as an important factor of having distortion from ideal geometry. Another important reason for distortion is the steric effect rendered by the presence of two methyl groups in each pyrimidyl ring. This type of *tris*-pyridyl/pyrimidyl chalcogenolate complexes of bismuth, *viz.*, $Bi(Sepy)_3$ and $Bi\{Sepy(Me\text{-}3)\}_3$ have previously been reported.[29] However, due to no or negligible steric interference, these complexes adopt monomeric structure. In the present case, it would be harmless to assume that the bulky nature of the ligands compels the third ligand to connect to two neighbouring Bi centres to finally yield a 1D coordination polymer. Similar type of polymeric Bi(III) chalcogenolate complex containing pyridyl moiety; $[Bi(\kappa^2\text{-S,N-pyS})_2(\mu\text{-S,N-pyS})]$ can also be found in literature.[30]

The axial Bi–S bond distances Bi–S(1A) = 2.5837 Å is comparable with reported values, whereas the equatorial Bi–S(1B) and Bi–S(1C) are elongated as compared to axial ones. This kind of feature can be observed in other complexes as well.[26,29,31] The Bi–N(2A) bond distance 2.7526(17) Å are significantly longer than those reported in literature *i.e.*, 2.5815(5) Å in $[Bi(1\text{-MMTZ})_2\{(PYM)(PYM(H))_2\}]$.[32] In the complex **1**, the Bi–N(2B) and Bi–N(1C) bond distances 2.952 and 2.962 Å can be considered as a weak interaction since their values are less than sum of the Van der Waals radii (3.62 Å).[29] All three S(1A)–C(1A), S(1B)–C(1B) and S(1C)–C(1C) bond distances (1.75 Å) are well anticipated in the literatures which reflect the existence of single bond character hence, confirms the predominance of thiol form over the thione form.[32]

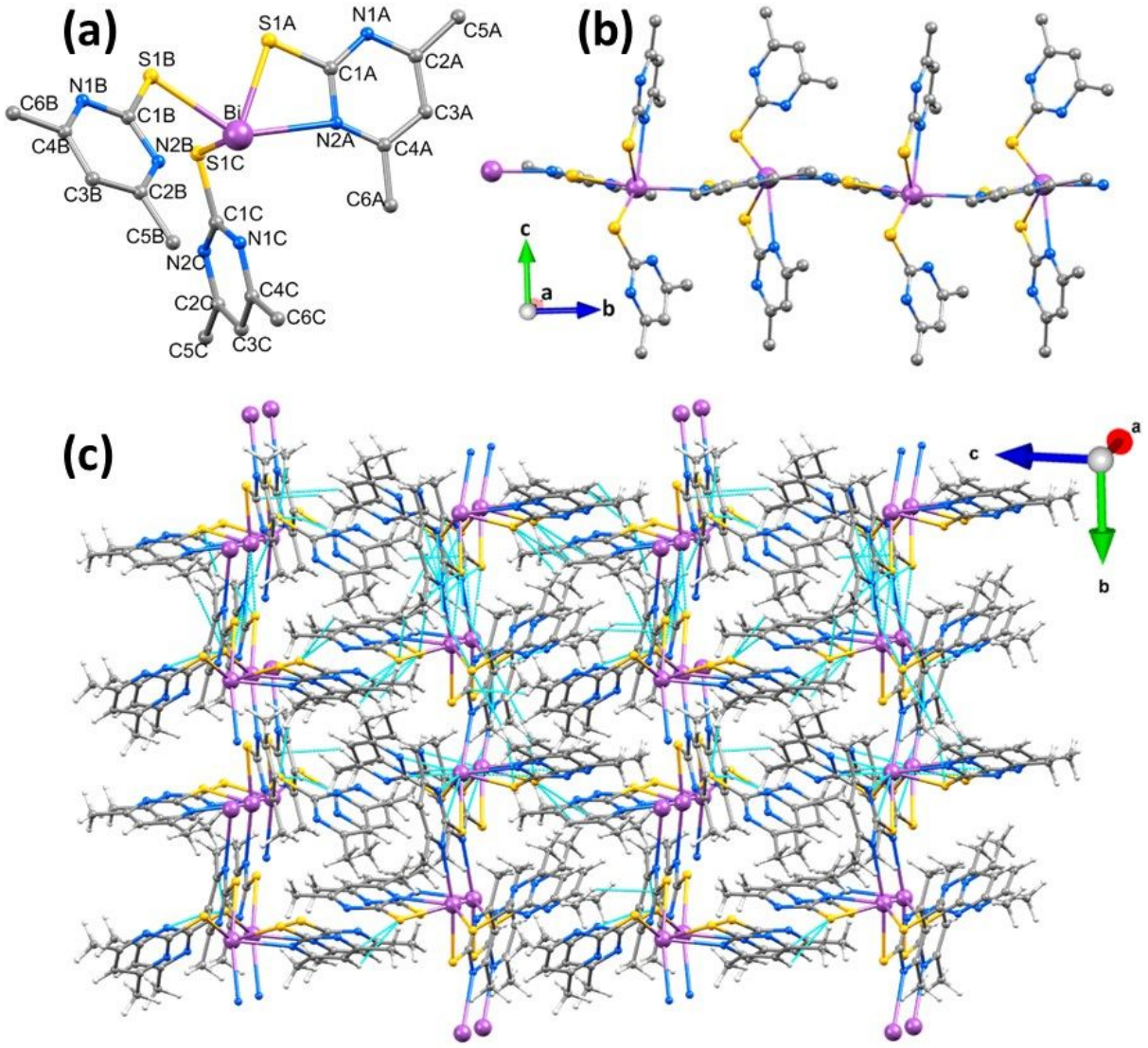

Fig. 2. (a) Molecular structure, (b) 1D polymeric chain and (c) packing diagram of $[Bi(4,6\text{-}Me_2pymS)_3]_n$ (**1**)

Table 1. Crystallographic and structural determination data for $[Bi(4,6\text{-}Me_2pymS)_3]_n$ (**1**)

Complex	$[Bi(4,6\text{-}Me_2pymS)_3]_n$
Chemical formula	$C_{18}H_{21}N_6S_3Bi$
Formula weight	626.57
Crystal size (mm^3)	0.1 × 0.05 × 0.025
Temperature/K	100(2)
Wavelength (Å)	0.41328
Crystal system	orthorhombic
Space group	$P\,2_1\,2_1\,2_1$
Unit cell dimensions	
a(Å)	10.9192(3)
b(Å)	10.9751(3)

c(Å)	18.2572(5)
α(°)	90
β(°)	90
γ(°)	90
Volume (Å^3)	2187.93 (10)
$\rho_{calcd.}$ (Mg/m^3)	1.902
Z	4
μ (mm^{-1})/ F(000)	2.086/ 1208
Limiting indices	-19 ≤ h ≤ 19
	-15 ≤ k ≤ 15
	-32 ≤ l ≤ 32
Θ for data collection (°)	1.530-22.831
No. of reflections collected	70,021
No. of independent reflections (R_{int})	11,465(0.0510)
Data/restraints/parameters	11465/0/260
Final R_1, wR_2 indices [I>2σI]	0.0157, 0.0352
R_1, wR_2 (all data)	0.0159, 0.0352
Goodness of fit on F^2	1.044

Thermal Studies

Analysis of the thermal behavior of any coordination complex is of utmost importance, especially when the latter is intended to be utilized a single source molecular precursor. The experiment was performed on crystalline sample in the temperature range 50–800 °C under N_2 atmosphere with a heating rate of 10 °C min^{-1}. From the TG profile of **1** (Fig. 3), it can be inferred that the complex is stable up to ~ 310 °C, after which the complex collapse via two step decomposition. The first step prompt decomposition (observed ~ 18.1%) corresponds to the formation of Bi_2S_3 (calculated ~ 18.2%). A gradual weight loss upto 800 °C was observed and the final weight loss (observed ~ 48%) does not corresponds to any composition of bismuth sulfide. It is well reported in literature that due the volatile nature and possibility of sublimation at an elevated temperature in group V metal sulfides (V-VI materials) restrict the exact determination of the nature of residue on the basis of weight loss percentage calculations.[26] Another plausible reason behind this type of gradual weight loss is the polymeric nature of the complex, which is quite commonly observed for coordination polymers and MOFs as given in literature.[33]

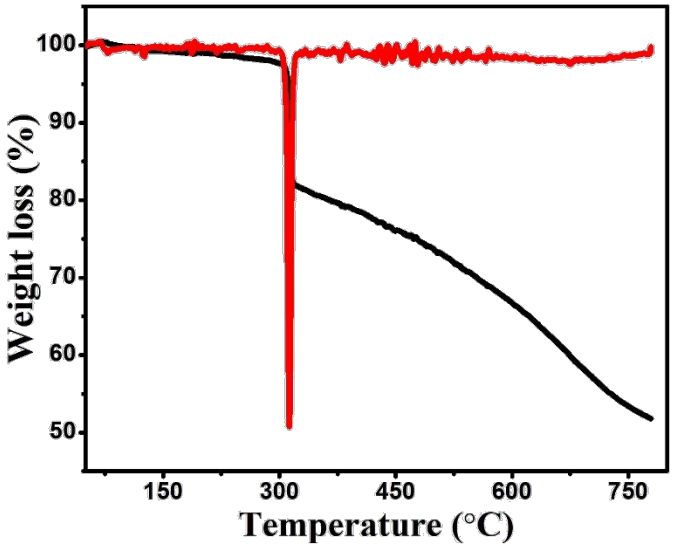

Fig. 3. Thermogravimetric analysis (TGA) curve for $[Bi(4,6\text{-}Me_2pymS)_3]_n$ (**1**).

Preparation and characterization of bismuth sulfide nanostructures

The thermal analysis of **1** has proved that the complex can be utilized as a suitable single source precursor for the preparation of bismuth sulfide materials. To further validate this claim, thermolysis of the complex was performed by heat-up method in oleylamine (OAm). The selection of solvent was done based on the fact that OAm have a high boiling point (350 °C) and acts as strong capping agent. Moreover, OAm being liquid at room temperature makes the purification procedure of the final product hassle-free. OAm is also known to facilitate the decomposition of the precursor by catalysing the process, thereby bringing down the decomposition temperature also, as compared to the TGA process.[34] Well separated nucleation and growth step are promoted in OAm which leads to the formation of monodispersed nanoparticles.[35] Revaprasadu *et al*. have reported the synthesis of antimony selenide nanorods in OAm at relatively lower temperature.[36] For temperature optimization, the complex was first heated in OAm in a heat-up fashion to point out the minimum decomposition temperature. It was found that the complex decomposes at very low temperature of 130 °C. The reaction was continued for 10 minutes. The PXRD pattern of the material isolated (Fig. 4b) was closely matching with phase pure orthorhombic Bi_2S_3 (bismuthinite) (ICSD Coll. Code 30775, Space group: P_{bnm}). The PXRD pattern, however, reveals the predominant formation of only (211) and (150) plane of the materials at 2θ = 26.0 and 46.6° respectively with highly amorphous nature (**BS1**). Thus, it was considered worthwhile to increase the reaction duration with the same temperature in order to

investigate the effect of time on the crystallinity of Bi_2S_3. Accordingly, decomposition at 130 °C was performed with 30 minutes reaction time (**BS2**). The PXRD pattern as shown in Fig. 4c show similar amorphous nature as observed in **BS1**. Thus, the increase in reaction duration do not seem to have drastic effect on the crystallinity of the material, a minute improvement, however was evident with a recognizable (231) plane in the latter case at 2θ = 52.8°. In the third set of reaction, the reaction temperature was increased to 160 °C and duration of 10 minutes was considered (**BS3**). The reflections originated from the PXRD pattern of **BS3** can be exactly matched with the same originating from the (002), (012), (022), (011), (111), (210), (211), (122), (130), (131), (024), (123), (104), (114), (002), (150), (231) and (242) planes of orthorhombic Bi_2S_3 material (Fig. 4d). The strong and sharp PXRD peaks in case of **BS3** indicates high crystallinity of Bi_2S_3. In all the cases, PXRD pattern does not contain any other reflections from any other phase of bismuth sulfide which confirm the phase purity of the nanostructures in all the three cases, while the broadening of the peaks are indicative of nano-sized particle formation. The average crystallite size calculated from the Scherrer equation[37] was found to be ~9, 11.3 and 26 nm for **BS1**, **BS2** and **BS3** respectively. It is important to mention that the Scherrer equation is often used to estimate the average crystallite size by correlating the scattering domain size and the FWHM (peak broadening) in the PXRD pattern. However, other factors like crystal distortion and defect formation are not considered in the equation.

2D elemental mapping is a quality tool to understand the distribution of constituent elements in any material. The 2D presented in Supplementary information Fig. S1 shows that Bi and S are distributed uniformly within the nanostructures. To gain better insight into the composition of the as prepared bismuth sulfide nanomaterials, EDS analysis was carried out (Supplementary information Fig. S2). The EDS spectra revealed that the atomic ratio of Bi and S is 39.8:60.2 (2:3.02), 38:62 (2:3.2) and 59.9:40.1 (3:2) for **BS1**, **BS2** and **BS3** respectively confirming the formation of Bi_2S_3 in each case.

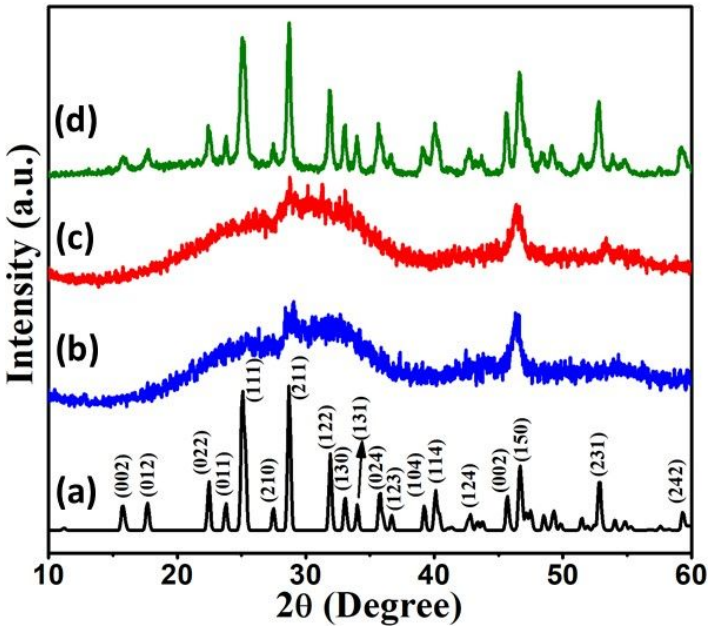

Fig. 4. (a) Simulated X-ray powder pattern (PXRD) of orthorhombic Bi_2S_3 (ICSD Coll. Code 30775). PXRD patterns of Bi_2S_3 synthesized at (b) 130 °C, 10 min (**BS1**), (c) 130 °C, 30 min (**BS2**) and (d) 150 °C, 10 min (**BS3**).

Raman spectroscopy is an ideal technique to investigate the phase purity along with the local site symmetry of any nanostructures. Moreover, Raman spectroscopy provides direct insight about the vibrational properties of any crystalline material. Thus, Raman spectroscopy was employed to characterize the Bi_2S_3 nanostructures. The Raman spectra reveals single vibrational mode peak at 235.8, 236.1 and 235.9 cm^{-1} for **BS1**, **BS2** and **BS3** respectively, (Fig. 5) which matches perfectly with the characteristic of A_g phonon mode for Bi_2S_3 material as reported in literature.[38] From the spectrum, it is also seen that there are slight shift in the Raman peak positions among the Bi_2S_3 nanostructures, which is the manifestation of the nano-size effects.[39] Furthermore, as the particle size of the Bi_2S_3 nanostructures increases from **BS1**, to **BS3**, a consistent increase in peak broadening (FWHM) is evident which is often observed for materials in nano-regime and happens due to lattice expansion, confinement of phonon and enhanced phonon-phonon interactions as reported in literature.[40]

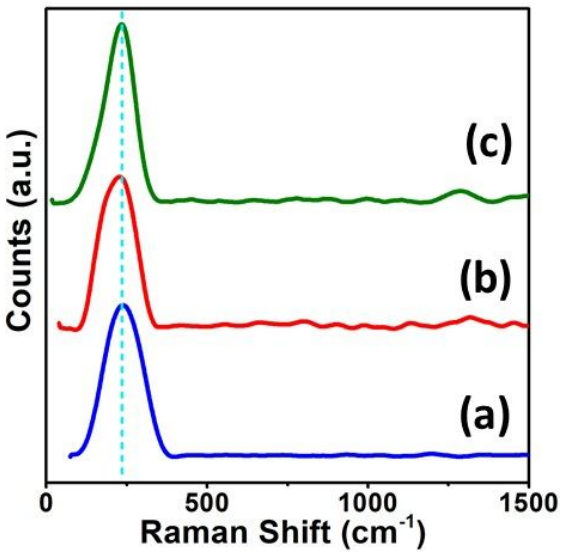

Fig. 5. Raman spectrum of Bi_2S_3 synthesized at (a) 130 °C for 10 min (**BS1**), (b) 130 °C for 30 min (**BS2**) and (c) 150 °C, 10 min (**BS3**) respectively.

The morphology of the as prepared Bi_2S_3 nanostructures was investigated by electron microscopic techniques. The Fig. 6a represents the SEM images for **BS1**. When corroborated with the TEM images (Fig. 6d for **BS1**), depicts the formation of flocculants with ill-defined morphology. From the SEM and TEM images of **BS2** (Fig. 6b and e), which was synthesized at the same temperature but at longer duration, it is clearly seen that the material comprise of irregular nanoflakes. In both these scenarios, the HRTEM image represented in Fig. 6g and h for **BS1** and **BS2** respectively, shows the presence of lattice fringes with clear d-spacing of 3.04 Å, which can be indexed to the (150) plane of orthorhombic Bi_2S_3. Finally, the SEM micrograph of the bismuth sulfide synthesized at higher temperature (**BS3**) divulges the presence of uniformly distributed small “rice grain” shaped nanorods (Fig. 6c). The TEM image (Fig. 6f) further confirms the nanorod morphology. The corresponding HRTEM reveals a d-spacing of 2.93 Å, which is indexed to (111) plane (Fig. 6i). For the above discussion, interestingly, it can be realized that in the utilization of the precursor under study, size and morphology modulation in bismuth sulfide nanostructures can be effortlessly achieved with subtle variation in thermolysis conditions.

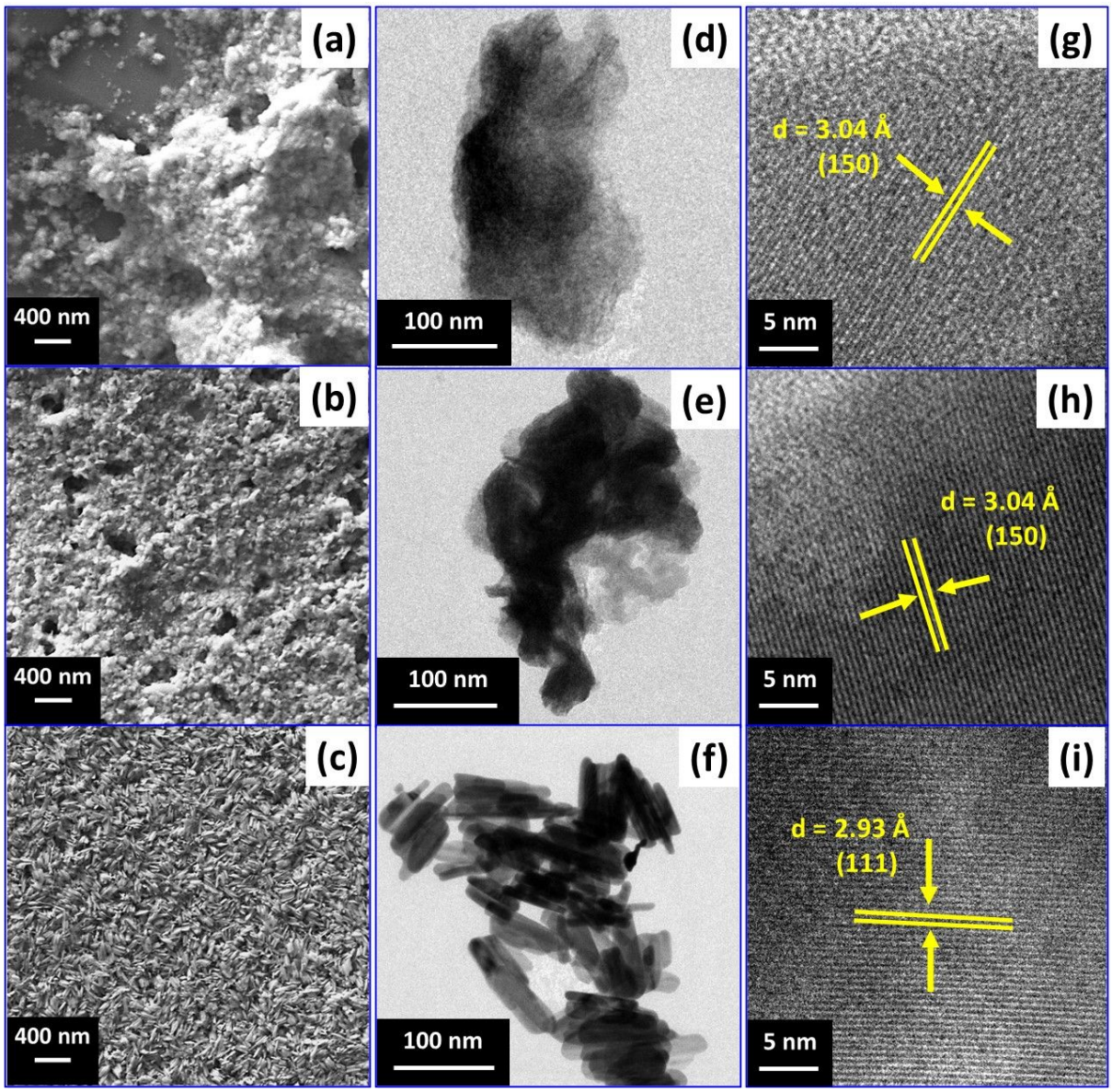

Fig. 6. (a,b,c) SEM micrographs, (d,e,f) TEM images and (g,h,i) HRTEM images of Bi_2S_3 synthesized at 130 °C for 10 min (**BS1**), 130 °C for 30 min (**BS2**) and 150 °C, 10 min (**BS3**) respectively.

Furthermore, the HRTEM images and the corresponding d-spacing values also support the growth of differently shaped bismuth sulfides. Xu *et al*., In a recent article, demonstrated that the preferential growth of bismuth sulfide material along (015) direction favours the formation of 2-dimensional morphology (nanoflakes in case of **BS2**).[41] A similar investigation by Sharma *et al.* have also led them to the same conclusion.[42] On the contrary, several studies, including a recent one from Onwudiwe's group[43] have proved that the formation of 1D nanostructure (nanorods in case of **BS3**) are evident when the growth is

directed along either (111) or (211) plane. The growth of 1-dimensional nanorods can be understood on the basis of orientation of Bi and S in the lattice. The lamellar arrangement of Bi^{3+} and S^{2-} in the infinite chains structure joined together by weak Bi-S bonds, imparts anisotropic nature in the structure. The crystal structure of Bi_2S_3 is composed of such infinite one-dimensional long chains which are interconnected by weak Van der Waals forces of attraction as shown in Fig. 7.[44] These weak interactions disappears at higher temperature (in present case 150°C) leading to the separation of chains which facilitate the formation of 1D nanostructures.[26]

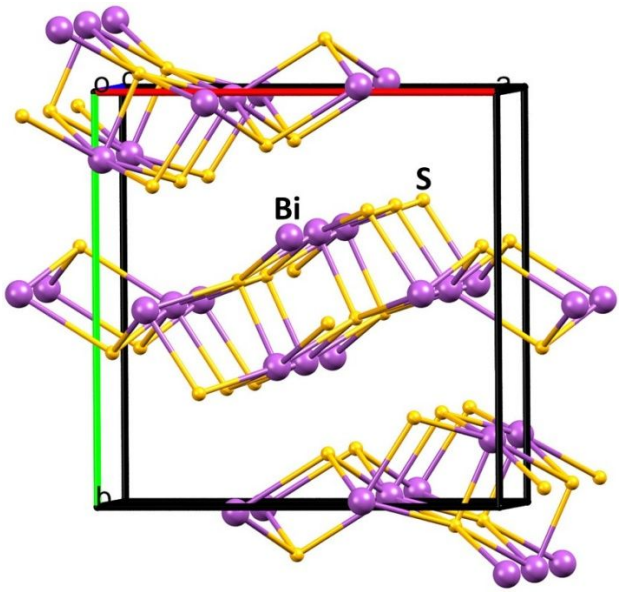

Fig. 7. Perspective view of crystal structure of orthorhombic Bi_2S_3 (ICSD Coll. Code 30775).

Optical Properties

Bismuth sulfide is a non-toxic crystalline n-type compound semiconductor belonging to V-VI semiconductor material family. Bulk Bi_2S_3 features a narrow band gap of 1.4 eV.[45] This feature of Bi_2S_3, when combined with its high absorption coefficient (10^{-4} to 10^{-6} cm^{-1})[46] project is as a fine candidate for optoelectronics, photovoltaics and good photocatalyst that is able to perform in the visible range of the solar spectrum. Keeping in mind the importance of optical band-gap in nanoelectronics, the optical properties of Bi_2S_3 nanostructures were investigated by diffuse reflectance spectroscopy (DRS) and the optical band gaps of these materials were determined by plotting the Kubelka–Munk function, F(R) as given in the following equation:

$[F(R)hv]^n = A(hv - Eg)$

Where hv is photon energy, A is a constant, Eg denotes the band gap, and n depends on the nature of the optical transition. The direct band gap of the materials was calculated using Tauc's model (n = 2).

From the diffuse reflectance spectra given in Fig. 8, it is observed that the direct optical band gaps of Bi_2S_3 nanostructures are 2.15, 2.00 and 1.93 eV for **BS1**, **BS2** and **BS3** respectively. These values are clearly blue shifted with respect to bulk band gap. The tunability in the band gap value in the as prepared nanostructures is a function of the increasing average crystallite size as we move from **BS1** to **BS3** since it is well known fact that with increasing size, optical band gap decreases.[47] The probable reason for the blue shift of the band gaps may be lattice distortions or surface lattice defects or quantum confinement or surface effect of the carriers.[48]

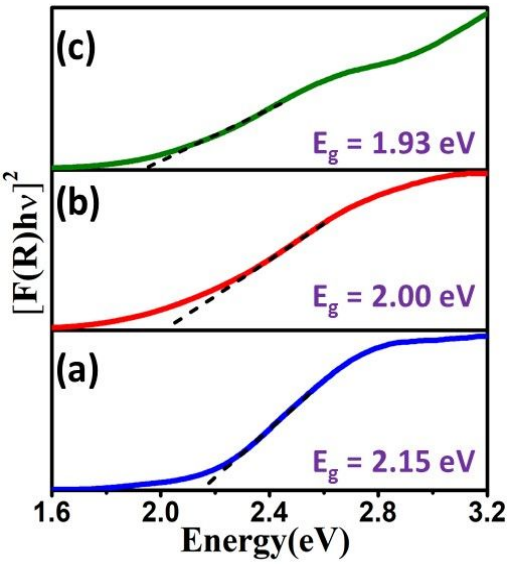

Fig. 8. Plots of $[F(R)hv]^2$ vs. energy generated by Kubelka–Munk transformation of solid-state diffuse reflectance data ofBi_2S_3 synthesized at (a) 130 °C for 10 min (**BS1**), (b) 130 °C for 30 min (**BS2**) and (c) 150 °C, 10 min (**BS3**) respectively.

Considering the fact that Bi_2S_3 has a large excitonic Bohr radius (r_B) ~24 nm,[49] and that the average crystallite size of **BS1** and **BS2** are lower than the above value, it would be harmless to consider the presence of quantum confinement effect in **BS1** and **BS2**.However, in case of **BS3**, due to its large average size, the presence of quantum confinement can be

ruled out and the observed blue shift in optical band gap may be attributed to lattice distortion or surface lattice defect. Nevertheless, the correlation between the size and optical band gap observed in the current study are in agreement with literature reports. For instance, Xiao *et al*. have reported a band gap of 1.9 eV for Bi_3S_3 nanorods having average diameter of ~15 nm.[50] In a separate study, Gao *et al*. have fabricated morphology controlled Bi_3S_3 nanostructures with band gap tunability. They have isolated hexagonal plates, mesocrystalline sheet and nanowires of Bi_3S_3 having optical band gap of 1.54, 1.73 and 1.96 eV respectively.[51]

Furthermore, the density of states and band structure of Bi_3S_3 was calculated considering conventional unit cell containing 20 atoms (8 Bi, 12 S) (Supplementary information Fig. S3). Fig. 9a presents the calculated projected density of states (PDOS) and band structure and of Bi_2S_3. The calculated band gap is found to be around 1.25 eV which is quite close to the experimentally observed value of Bulk Bi_2S_3 (~ 1.4 eV).[45] The valance band maxima (VBM) and conduction band minima (CBM) are located along Γ-Y/ Γ-X directions (Fig. 9b). The PDOS near valance band maxima is consist of majorly S-3p orbitals along with minor contributions from Bi-6s, Bi-6p states. In contrast, the conduction band minima have major contributions from mixed states of Bi-6p, S-3s and S-3p orbitals. Overall, S-state dominates the VBM while Bi-states dominate in the CBM. Thus, optical transition from valance to conduction band is expected to originate from S-state and finish in Bi-states, which is consistent with the fact that each Bi is surrounded by seven S atoms withing the 3.4 Å separation.

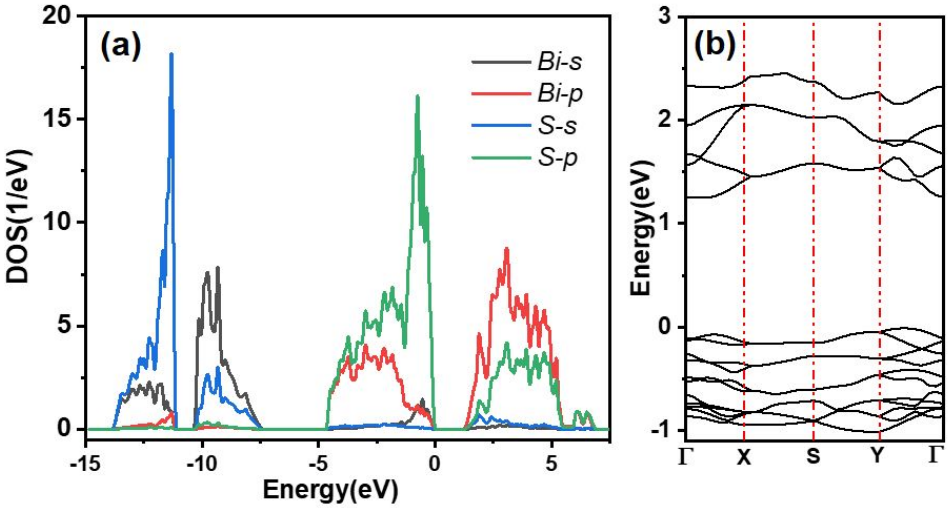

Fig. 9. (a) Projected density of states and (b) band structure of Bi_2S_3.

Photo-response and photo-switching study of Si/Bi_2S_3 liquid junction photoelectrochemical cells

Bi_2S_3 is one of the earliest materials known to exhibit photo conducting properties.[6] The Photo-response and photo-switching behaviour of the as-prepared Bi_2S_3 has been evaluated by fabricating prototype photoelectrochemical (PEC) cells with a three-electrode system. The working electrode was fabricated by spin coating a colloidal suspension of Bi_2S_3 nanomaterials in toluene over a Si substrate followed by evaporation of the solvent to give a thin film of the material. Experimental details are provided in supporting information.

In the present work, since phase pure Bi_2S_3 have been isolated in all the three reactions, **BS3** was selected as a representative material keeping in mind the good crystallinity and band gap, and Photo-response and photo-switching of this material was investigated. The current-voltage (I–V) measurement for Si/Bi_2S_3 cell shows a nonlinear characteristic when irradiated in the presence of Na_2S and Na_2SO_3 as electrolyte (Fig. 10a). On illuminating with light source (200 μW cm^{-2}), the energy from the light excites the electrons in the semiconductor Bi_2S_3 from the valence band into the conduction band. This increase in availability of electrons results in increased photoconductivity (Fig. 10b) shows the photo response as a function of time when the lamp was switched on and off. The cell shows no further change in current on exposing to light after considerable amount of time which indicates saturation process. When the light was turned off, the “carrier generation process” abruptly stops while the “carrier loss process” carries on, resulting in a sudden decrease in the conductivity.[52] Thus, the cell made from Bi_2S_3 nanomaterial, under dark and light condition shows good photo switching and photostability between low and high conductivity. Guo *et al.* reported earlier that resistive switching in Bi_2S_3 occurs due to its specific intrinsic doping with sulfur vacancies and hence exhibits great potential for application in resistive memory devices.[53] Here on applying bias voltage of -1.5 V, the photocurrent ($I_{pc} = I_{light} - I_{dark}$) found to be ~5 μA while in an earlier report, Bi_2S_3 nanowire synthesized by Bao *et al.* using hydrothermal method shows photocurrent of ~60 nA and ~20 nA when illuminated by green laser and the quartz lamp as light sources, respectively and bias voltage of 3 V.[54] Later, Xiao *et al.*[50] reported Bi_2S_3 hierarchical architectures which

exhibited improved photocurrent ~28 μA on applying bial volatage of 5V, which is significantly higher compared to bias voltage used in present study. Photoresponsivity is the photocurrent generation efficiency of any material and can be expressed by the ratio of generated photocurrent and incident optical power ($R = I_{pc}/PS$)[55] (P = 200 μW cm^{-2} and the effective area of the cell; S = 0.785 cm^2 in the present case). In this study, the photoresponsivity was calculated to be 31 mAW^{-1}. From the repeated cycles, the middle cycle has been chosen to calculate the rise time (the time required for the current to increase from 10% to 90% of the peak value) and fall time in each case. The rise and fall times for **BS3** are 2 s indicating fast response (Fig. 10c). It is to be noted that the rise and fall time are the same in this case, which indicates involvement of less trap states or defects in the switching process.[56] The fast switching characteristics along with good photoresponsivity obtained in the present study for Bi_2S_3 nanorods proves their candidature for low-cost alternative photon absorber material for solar cell as well as efficient material for photodetectors and optical switches.

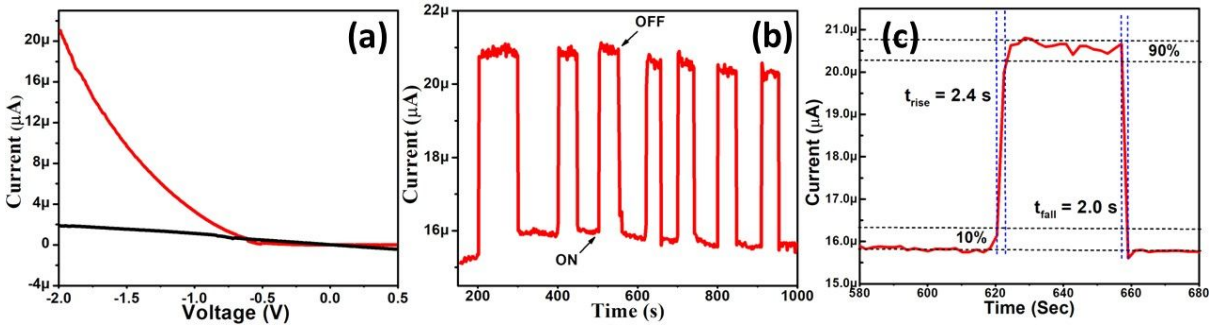

Fig. 10. (a) I-V characteristics, (b) reversible switching behaviour under alternating light and dark conditions and (c) expanded view of the middle cycle of the pristine Bi_2S_3 nanorods synthesized at 150 °C, 10 min (**BS3**).

Conclusion

This account describes the successful room temperature synthesis and structural characterization of stable bismuth-dimethylpyrimidylthiolate molecular precursor for Bi_2S_3 nanostructures. Notably, the three dimethylpyrimidylthiolate ligand attached to bismuth centre exhibit different kind of coordination behavior which leads to the isolation of 1D $[Bi(\kappa\text{-S,N-pymS})(pymS)(\mu\text{-S,N-pymS})]_n$ polymeric chain. The complex underwent facile thermal transformation to afford phase pure Bi_2S_3 nanostructure at low temperatures in

OAm. Interestingly, the reaction temperature was significantly lower than the decomposition temperature of the complex as determined by TGA. This clearly reflects that OAm not only serves as capping agent for the nanostructures but also catalyze the decomposition of the precursor. Additionally, the investigation also highlighted the significant influence of the reaction temperature on the phase formation, morphology and bandgap of nanostructures. The estimated bandgaps of nanostructures were blue shifted with respect to the bulk bandgap and are in the range suitable for solar cell application. Furthermore, the prototype photo-electrochemical cell fabricated from the pristine Bi_2S_3 nanostructures exhibited remarkable photoresponsivity and photostability under alternating light and dark conditions. Overall, this report presents a facile and scalable route to Bi_2S_3 nanostructures at relatively low temperature with the liberty of tuning morphology and bandgap. Similar approach can be explored for other metals to develop efficient precursors in future for the preparation of high quality metal chalcogenide nanostructures.

Supplementary Information

Electronic Supplementary Information (ESI) available: [Additional figures etc.]. CCDC-No. 2210360 for $[Bi(4,6\text{-}Me_2pymS)_3]_n$ contains the supplementary crystallographic data for this paper. This data can be obtained free of charge at www.ccdc.cam.ac.uk/conts/retrieving.html or from the Cambridge Crystallographic Data Centre, 12 Union Road, Cambridge CB2 1EZ, UK [Fax: +44-1223/336-033; E-mail: deposit@ccdc.cam.ac.uk].

Conflicts of interest

The authors declare no conflicts of interest.

Acknowledgements

We thank Dr A. K. Tyagi, Director, Chemistry Group, Bhabha Atomic Research Centre for the encouragement of this work. We also thank Dr Bal Govind Vats (Fuel Chemistry Division, Bhabha Atomic Research Centre) for TG and PXRD measurements. RJB acknowledge sincere gratitude to Advanced Photon Source (APS) located at Argonne National Laboratory for mounting the crystal at their facility. Chem Mat CARS Sector 15 is supported by the National Science Foundation under grant number NSF/CHE-1834750. This research used resources of

the Advanced Photon Source; a U. S. Department of Energy (DOE) Office of Science User Facility operated for the DOE Office of Science by Argonne National Laboratory under Contract No. DE-AC02-06CH11357.

References:

1. A. Swarnkar, W. J. Mir, R. Chakraborty, M. Jagdeeswararao, T. Sheikh and A. Nag, *Chem. Mater*., 2019, **31**, 565-575.
2. D. Wang, F. Yin, Z. Du, D. Han and J. Tang, *J. Mater. Chem. A*, 2019, **7**, 26205-26226.
3. G. Karmakar, A. Tyagi, A. P. Wadawale, A. Y. Shah, G. Kedarnath, A. P. Srivastava and V. Singh, *J. Mater. Sci*., 2020, **50**, 15439-15453.
4. A. A. Tahir, M. A. Ehsan, M. Mazhar, K. G. U. Wijayantha, M. Zeller and A. D. Hunter, *Chem. Mater*., 2010, **22**, 5084-5092.
5. W. M. Linhart, S. J. Zelewski, P. Scharoch, F. Dybala and R. Kudrawiec, *J. Mater. Chem. C*, 2021, **9**, 13733-13738.
6. M. Bernechea, Y. Cao and G. Konstantatos, *J. Mater. Chem. A*, 2015, **3**, 20642-20648.
7. J. Chen, S. Qin, G. Song, T. Xiang, F. Xin and X. Yin, *Dalton Trans*., 2013, **42**, 15133-15138.
8. C. Nithya, J. K. R. Modigunta, I. In, S. Kim and S. Gopukumar, *ACS Appl. Nano Mater*., 2023, **6**, 6121-6132.
9. L. X. Hao, G. Chen, Y. G. Yu, Y. S. Zhou, Z. H. Han and Y. Liu, *Int. J. Hydrog. Energy*, 2014, **39**, 14479-14486.
10. M. P. Motaung, D. C. Onwudive and W. Lei, *ACS Omega*, 2021, **6**, 18975-18987.
11. B. Sun, T. Feng, J. Dong, X. Li, X. Liu, J. Wu and S. Ai, *CrystEngComm*, 2019, **21**, 1474-1481.
12. V. Brune, M. Grosch, R. Weibing, F. Hartl, M. Frank, S. Mishra and S. Mathur, *Dalton Trans*., 2021, **50**, 12365-12385.
13. D. C. Onwudiwe and V. M. Nkwe, *Heliyon*, 2020, **6**, e04505.
14. W. N. Kun, S. Mlowe, L. D. Nyamen, M. P. Akerman, P. O'Brien, P. T. Ndifon and N. Revaprasadu, *Polyhedron*, 2018, **154**, 173-181.
15. W. N. Kun, S. Mlowe, L. D. Nyamen, P. T. Ndifon, M. A. Malik, O. Q. Munro and N. Revaprasadu, *Chem. Eur. J*., 2016, **22**, 13127.

16. W. N. Kun, P. D. McNaughter, L. D. Nyamen, B. F. Spencer, P. O'Brien, P. T. Ndifon and N. Revaprasadu, *RSC Adv*., 2019, **9**, 15836-15844.
17. O. C. Monteiro, T. Trindade, J. H. Park and P. O'Brien, *Chem. Vap. Depos*., 2000, **6**, 230-232.
18. Q. Han, J. Chen, X. Yang, L. Lu and X. Wang, *J. Phys. Chem. C*, 2007, **111**, 14072-14077.
19. L. Tian, H. Y. Tan and J. J. Vittal, *Cryst. Growth Des*., 2008, **8**, 734-738.
20. J. L. T. Chen, V. Nalla, G. Kannaiyan, V. Mamidala, W. Ji and J. J. Vittal, *New J. Chem*., 2014, **38**, 985-992.
21. T. Alqahtani, M. D. Khan, D. J. Kelly, S. J. Haigh, D. J. Lewis and P. O'Brien, *J. Mater. Chem. C*, 2018, **6**, 12652-12659.
22. W. Lou, M. Chen, X. Wang and W. Liu, *Chem. Mater*., 2007, **19**, 872-878.
23. M. Y. Masoomi and A. Morsali, *Coord. Chem. Rev*., 2012, **256**, 2921-2943.
24. K. J. Lee, J. H. Lee, S. Jeoung and H. Moon, *Acc. Chem. Res*., 2017, **50**, 2684-2692.
25. G. Karmakar, A. Tyagi, K. K. Halankar, S. Nigam, B. P. Mandal, A. P. Wadawale, G. Kedarnath and A. K. Debnath, *Dalton trans*., 2023, **52**, 1461-1475.
26. A. Thomas, G. Karmakar, A. Y. Shah, S. V. Lokhande, A. Y. Kulkarni, A. Tyagi, R. S. Chauhan, N. N. Kumar and A. P. Singh, *Dalton Trans*., 2022, **51**, 12181-12191.
27. G. Karmakar, A. Tyagi, A. Y. Shah, S. Nigam, A. P. Wadawale, G. Kedarnath, B. G. Vats, N. N. Kumar and V. Singh, *Dalton Trans*., 2022, **51**, 12670-12685.
28. A. Tyagi, G. Karmakar, B. P. Mandal, D. D. Pathak, A. Wadawale, G. Kedarnath, A. P. Srivastava and V. K. Jain, *Dalton Trans*., 2021, **50**, 13073-13085.
29. R. K. Sharma, G. Kedarnath, V. K. Jain, A. Wadawale, M. Nalliath, C. G. S. Pillaia and B. Vishwanadh, *Dalton Trans*., 2010, **39**, 8779-8787.
30. E. Wächtler, R. Gericke, T. Block, B. Gerke, R. Pöttgen and J. Wagler, *Z. Naturforsch. B*., 2021, **76**, 103-118.
31. E. Block, G. O. Okai, H. Kang, J. Wu and J. Zubieta., *Inorg. Chem*., 1991, **30**, 4784-4788.
32. A. Luqman, V. L. Blair, R. Brammananth, P. K. Crellin, R. L. Coppel and P. C. Andrews., *Eur. J. Inorg. Chem*, 2016, **2016**, 2738-2749.
33. A. Walczak, G. Kurpik and A. R. Stefankiewicz, *Int. J. Mol. Sci*., 2020, **21**, 6171.
34. S. Mourdikoudis and L. M. L. Marzan, *Chem. Mater*.,2013, **25**, 1465-1476.
35. Y. C. Cao and J. Wang, *J. Am. Chem. Soc.*, 2004, **126**, 14336-14337.

36. M. D. Khan, M. Aamir, M. Sohail, M. Sher, J. Akhtar, M. A. Malik and N. Revaprasadu, *Solar Energy*, 2018, **169**, 526-534.
37. P. Scherrer, *Nachr. Ges. Wiss. Goettingen, Math.-Phys. Kl*., 1918, **2**, 98-100.
38. M. P. Deshpande, P. N. Sakariya, S. V. Bhatt, N. H. Patel, K. Patel and S. H. Chaki, *Bull. Mater. Sci*., 2015, **38**, 83-88.
39. U. V. Ghorpade. M. P. Suryawanshi, S. W. Shin, I. Kim, S. K. Ahn, J. H. Yun, C. Jeong, S. S. Kolekar and J. H. Kim, *Chem. Mater.*, 2016, **28**, 3308-3317.
40. O. A. Yassin, S. N. Alamri and A. A. Joraid, *J. Phys. D: App. Phys.*, 2013, **46**, 235301.
41. X. Xu, C. Ye, D. Chao, B. Chen, H. Li, C. Tang, X. Zhong and S.-Z. Qiao, *Adv. Mater.*, 2022, **34**, 2108688.
42. A. Sharma, B. Bhattacharyya, A. K. Srivastava, T. D. Senguttuvan and S. Husale, *Sci. Rep*., 2016, **6**, 19138.
43. T. O. Ajiboye and D. C. Onwudiwe, *Results in Chemistry*, 2021, **3**, 100151.
44. C. Li, J. Zhao, Q. Hu, Z. Liu, Z. Yu and H. Yan, *J. Alloys Compd*., 2016, **688**, 329-335.
45. T. O. Ajiboye, O. A. Oyewo and D. C. Onwudiwe, *Surf. Interfaces*, 2021, **23**, 100927.
46. T. Fazal, S. Iqbal, M. Shah, A. Bahadur, B. Ismail, H. S. M. Abd-Rabboh, R. Hameed, Q. Mahmood, A. Ibrar, M. S. Nasar, Y. Ehsan, A. N. S. Saqib, Adnan and M. A. Qayyum, *J. Mater. Sci.: Mater. Electron.*, 2022, **33**, 42-53.
47. G. Karmakar, A. Tyagi, A. Wadawale, G. Kedarnath, A. P. Srivastava, C. A. Betty and V. Singh, *ChemistrySelect*, 2018, **3**, 10394-10401.
48. G. Karmakar, D. D. Pathak, A. Tyagi, B. P. Mandal, A. Wadawale and G. Kedarnath, *Dalton Trans*., 2023, **52**, 6700-6711.
49. E. V. Guimarães, E. R. Gonçalves, S. A. Lourenço, L. C. Oliveira, O. Baffa, A. C. A. Silva, N. O. Dantas and R. S. Silva, *J. Alloys Compd.*, 2018, **740**, 974-979.
50. G. Xiao, Q. Dong, Y. Wang, Y. Sui, J. Ning, Z. Liu, W. Tian, B. Liu, G. Zou and B. Zou, *RSC Adv*., 2012, **2**, 234-240.
51. M.-R. Gao, S.-H. Yu, J. Yuan, W. Zhang and M. Antonietti, *Angew. Chem. Int. Ed*., 2016, **55**, 12812-12816.
52. G. Karmakar, A. Tyagi, A. Y. Shah, L. B. Kumbhare, A. P. Wadawale, G. Kedarnath and V. Singh, *RSC Adv*., 2022, **12**, 27292-27299.
53. D. Guo, C. Hu and C. Zhang, *Mater. Res. Bull*., 2013, **48**, 1984-1988.

54. H. Bao, X. Cui, C. M. Li, Y. Gan, J. Zhang and J. Guo, *J. Phys. Chem. C*., 2007, **11**, 12279-12283.

55. Q. Hao, J. Liu, G. Wang, J. Chen, H. Gan, J. Zhu, Y. Ke, Y. Chai, J. Lin and W. Zhang, *ACS Nano*, 2020, **14**,11373-11382.

56. G. Karmakar, A. Y. Shah, A. Tyagi, A. P. Wadawale, G. Kedarnath, N. N. Kumar and J. Bahadur, *New J. Chem*., 2022, **46**, 3871-3881.